



# Synthesis and antibacterial study of 2-amino-4*H*-pyrans and pyrans annulated heterocycles catalyzed by sulfated polysaccharide-coated BaFe<sub>12</sub>O<sub>19</sub> nanoparticles

Sara Amirnejat<sup>1</sup> · Aliakbar Nosrati<sup>1</sup> · Reza Peymanfar<sup>1</sup> · Shahrazad Javanshir<sup>1</sup>

Received: 4 February 2020 / Accepted: 27 April 2020  
© Springer Nature B.V. 2020

## Abstract

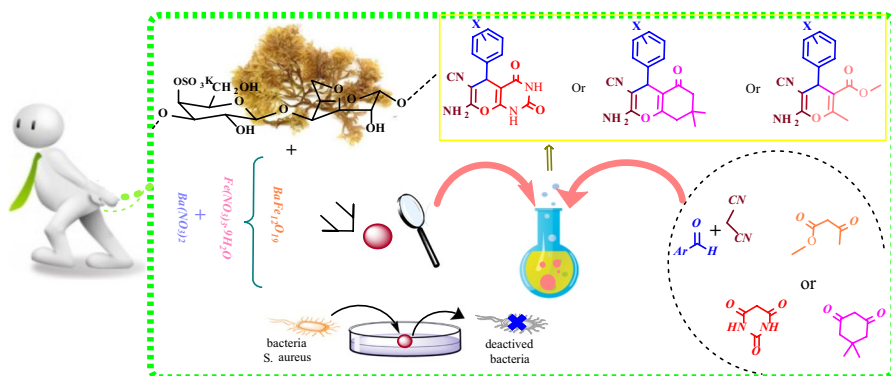
In this procedure, the synthesis of ecofriendly, magnetically retrievable BaFe<sub>12</sub>O<sub>19</sub> was reported using a sulfated polysaccharide of algal origin, Irish moss (IM), as bio-matrix and capping agent. The characterization of BaFe<sub>12</sub>O<sub>19</sub>@IM was performed by some physicochemical characterization tools, such as Fourier transform infrared spectroscopy, X-ray powder diffraction, scanning electron microscopy, energy-dispersive X-ray spectroscopy, vibrating sample magnetometer, and thermogravimetric analysis. The catalytic performance and recyclability of the introduced heterogeneous catalyst have been explored in the one-pot synthesis of 2-amino-4*H*-pyrans and pyrans annulated heterocyclic compounds via a three-component reaction between aldehydes, malononitrile, and various C–H activated acidic compound under green reaction conditions. This environmentally benign catalyst displayed high catalytic activity and effective reusability and could maintain its high catalytic efficiency even after six recycling runs. Furthermore, the antibacterial activity of BaFe<sub>12</sub>O<sub>19</sub>@IM and the selected compound (**4a**) toward two types of clinically isolated bacterial strains *Escherichia coli* (*E. coli*) and *Staphylococcus aureus* (*S. aureus*) was evaluated. The results revealed that BaFe<sub>12</sub>O<sub>19</sub>@IM and 2-amino-4-(4-chlorophenyl)-7,7-dimethyl-5-oxo-5,6,7,8-tetrahydro-4*H*-chromene-3-carbonitrile (**4a**) showed an effective antibacterial activity against gram-positive *S. aureus*.

---

✉ Sara Amirnejat  
shjavan@iust.ac.ir

<sup>1</sup> Heterocyclic Chemistry Research Laboratory, Department of Chemistry, Iran University of Science and Technology, 16846-13114 Tehran, Iran

## Graphic abstract



**Keywords** Biopolymer · Magnetic nanocomposite · Irish moss · 2-Amino-4H-pyran · Antibacterial activity

## Introduction

The accumulation of metallic nanoparticles in the environment could adversely affect the ecosystem [1–3]. Therefore, recycling and reuse of metal nanoparticles can prevent their accumulation and thus minimize their negative effects. Nevertheless, the separation and recycling of the metallic nanoparticles from the reaction medium persist a main defy [4]. Magnetically separable nanoparticles (MSNPs) [5] were employed as an appropriate solution to overcome sophisticated separation techniques, such as filtration or centrifugation [6, 7]. This type of nanomaterial can be effortlessly and rapidly separated from the reaction mixture using a simple magnet [8, 9]. As such, mixed, ferrimagnetic hexaferrites oxides, which are classified into six categories according to the chemical formulas and crystalline structures (M, Y, Z, W, X, and U types), are interesting materials that have aroused great interest [10, 11]. Meanwhile, M-type barium hexaferrite having a good combination of three advantages, namely high magnetic properties, chemical stability, and low cost, is considered as a good choice [12–14].

The utilization of polymer-coated magnetic particles as efficient nanocatalysts has been considered recently. Biopolymer coating of magnetic particles is of interest to overwhelm the aggregation [15]. The special polysaccharides which have been extracted from algal origin can be used as natural polymers coating agents [16–18]. In this case, red algae such as IM derived from the *Chondrus crispus* are extremely sulfated galactans [19, 20]. In this respect, these carbohydrates are mostly  $\kappa$ - and  $\iota$ -carrageenan with both sulfate and OH group reacting as double-acting catalyst.

Multi-component reactions (MCRs) [21, 22] are the series of special types of synthetically useful organic reactions in which three or more substrates react to give a final product in a one-pot procedure. Owing to an extensive range of MCRs

applications in different areas like the preparation of different structural scaffolds and the detection of new drugs, these types of reactions have drawn considerable attention in organic synthesis and pharmaceutical chemistry [23]. 4*H*-pyran derivatives are a remarkable category of heterocyclic compounds, due to their significant properties for the treatment of numerous neurodegenerative diseases, which include Parkinson, Alzheimer, Huntington, amyotrophic lateral sclerosis, AIDS-associated dementia, Down's syndrome, schizophrenia, and also cancer treatment [24–26]. Furthermore, other applications can be mentioned including, laser dyes [27], optical brighteners, pigment industries [28], and biodegradable agrochemicals properties [29]. As a result, numerous methods have been reported for the synthesis of 4*H*-pyrans in the presence of catalysts such as chitosan-CTAB [30], ZnFe<sub>2</sub>O<sub>4</sub>@ alginate acid [31], Fe<sub>3</sub>O<sub>4</sub>@xanthan gum [32], MCM-41@Schiff base-Co(OAc)<sub>2</sub> [33], Fe<sub>3</sub>O<sub>4</sub>@SiO<sub>2</sub>@TiO<sub>2</sub> [34], saccharose [35], and muskmelon fruit shell (WEMFSA) [36].

Nowadays, the resistance of microorganisms to various antibiotics has become one of the most serious global health problems [37–39]. The high prevalence of multidrug-resistant bacteria has put the effectiveness of these drugs in serious danger. These results indicate that increasing antibiotic resistance, which has always been one of the most important global health problems, is now an increasing threat, and the development of a new strategy to overcome this problem is urgently needed [40–42]. One of these strategies is the use of metallic nanoparticles. In recent years, there has been an unprecedented explosion of research on the use of metal-based nanostructures as antibacterial agents [43]. Metallic nanoparticles can affect bacteria through multiple mechanisms. The best known mechanisms are induction of oxidative stress, interaction and/or permeabilization of the cell membrane, generation of metal ions, interactions with proteins and/or with DNA [44].

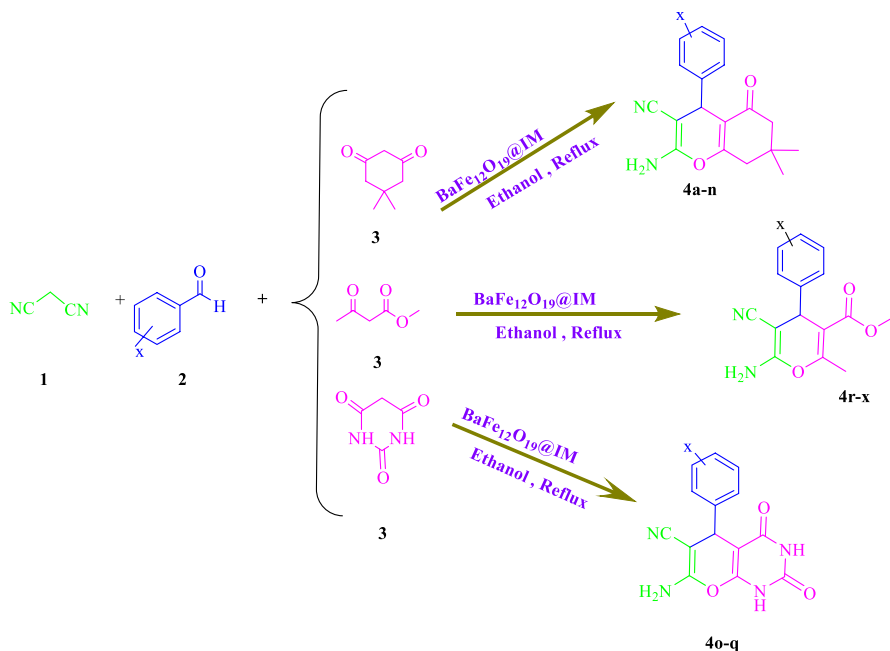
Pursuant to the above-mentioned statements, our research group introduce a new Irish moss-based nanocomposite, BaFe<sub>12</sub>O<sub>19</sub>@IM, which was successfully applied as a heterogeneous bifunctional catalyst for the synthesis of 4*H*-pyran derivatives via one-pot, three-component reaction between various aromatic aldehydes, malononitrile, and dimedone, methyl acetoacetate or malonylurea at room temperature in ethanol (Scheme 1).

In addition to the catalytic study, the antibacterial properties of BaFe<sub>12</sub>O<sub>19</sub>@IM were investigated on two bacterial strain, *S. aureus*, and *E. coli*. The results revealed good antibacterial activity against gram-positive *S. aureus*.

## Experimental

### Chemicals and materials

All materials were purchased from Merck and used without purification. IR spectra were recorded on KBr discs on a Shimadzu FT-IR-8400S spectrometer. X-ray diffraction (XRD) measurements were carried out using Philips X'Pert MPD analyzer (with a range of  $2\theta = 10\text{--}80$  degree on 40 kV current and 40 mA with wave length of  $\lambda = 1.78897 \text{ \AA}$  using Co tube). Calcination of catalyst was performed by Exciton



**Scheme 1.** Synthesis of 2-Amino-3-cyano-4*H*-pyrans by  $\text{BaFe}_{12}\text{O}_{19}@\text{IM}$

oven. A vibrating-sample magnetometer (VSM) model was recorded by MDKFD (Danesh Pajohan Kavir Co). Scanning electron microscope (SEM, Tescan Mira3) was used for analyses from Czech Republic. NMR spectra were recorded using a German Bruker Avance DRX 500 MHz instrument with  $\text{CDCl}_3$  solvent. Melting point was measured by Electrothermal 9100. Sonication for synthesis of catalyst was performed by Elma at 60 Hz. All thermogravimetric analyses were performed using a model STA504, BÄHR Thermoanalyse GmbH (Hüllhorst, Germany).

### Synthesis of barium hexaferrite ( $\text{BaFe}_{12}\text{O}_{19}$ ) magnetic nanoparticles

$\text{BaFe}_{12}\text{O}_{19}$  barium hexaferrite was prepared according to our previously reported method [32]. A mixture of barium nitrate ( $\text{Ba}(\text{NO}_3)_2$ ) (0.52 g, 1.99 mmol), iron(III) nitrate-nonahydrate ( $\text{Fe}(\text{NO}_3)_3 \cdot 9\text{H}_2\text{O}$ ) (9.6 g, 23.76 mmol), and 4.5 g of citric acid in 100 mL of double distilled water was sonicated in ultrasonic bath for 15 min. Aqueous ammonia solution (25%) was then added until the solution reaches pH 8. The obtained solids were filtered, washed, dried at 80 °C, and finally calcined at 750 °C for 2 h to furnish the desired barium hexaferrite magnetic nanoparticles.

### Synthesis of $\text{BaFe}_{12}\text{O}_{19}@\text{IM}$ nanocomposite

The Irish moss was washed several times with water to remove residual salts, filtered and dried at room temperature, and ground to obtain IM powder.

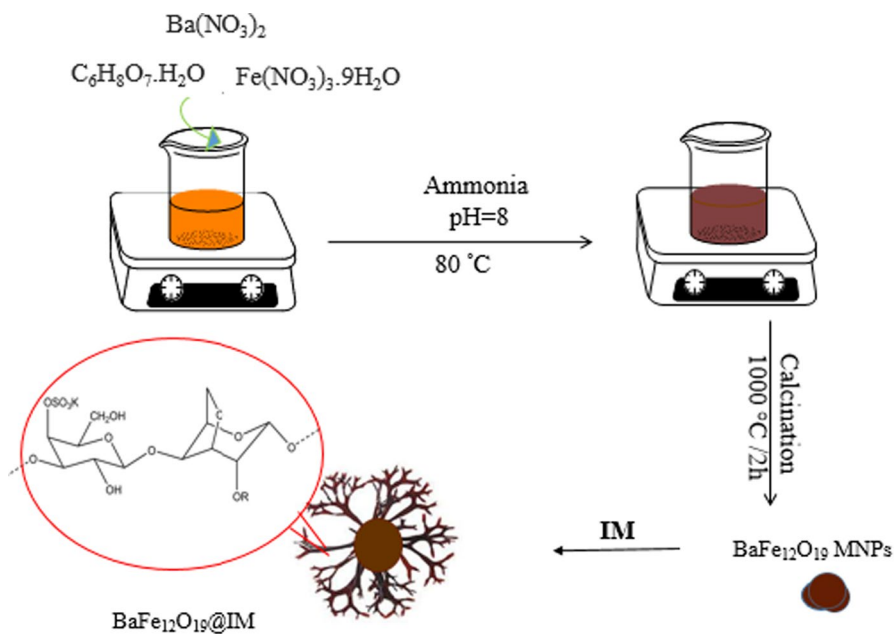
A mixture of IM powder (7.8 g) and BaFe<sub>12</sub>O<sub>19</sub> (3.12 g, 0.36 mmol) in 15 mL H<sub>2</sub>O: ETOH solvent mixture (2:1 volume ratio) was stirred for 2 h, followed by sonication in water bath for 40 min. The achieved product was separated by external magnet and oven-dried for 6 h to obtain BaFe<sub>12</sub>O<sub>19</sub>@IM nanocomposite (Scheme 2).

### General procedure for synthesis of pyran derivatives (4a–x)

A mixture of aromatic aldehydes (1 mmol), malononitrile (1 mmol), dimedone or malonylurea or methyl acetoacetate (1 mmol) and BaFe<sub>12</sub>O<sub>19</sub>@IM nanocomposite (12 mg) in ethanol (5 mL) was stirred under reflux condition until completion of the reaction which was monitored by TLC (eluent: EtOAc/*n*-hexane, 1:3). The catalyst was separated from the mixture by an external magnet, washed, and dried for use in the next run. The crude products were filtered and recrystallized from ethanol.

### Spectral data for some products

**2-Amino-4-(2,4-dichlorophenyl)-7,7-dimethyl-5-oxo-5,6,7,8-tetrahydro-4*H*-chromene-3-carbonitrile (4d)** pale yellow crystalline solid. m.p.: 180–183 °C. <sup>1</sup>HNMR (500 MHz, CDCl<sub>3</sub>, 25 °C): δ = 1.04 (s, 3H, CH<sub>3</sub>), 1.10 (s, 3H, CH<sub>3</sub>), 2.25 (s, 2H, CH<sub>2</sub>), 2.43 (s, 2H, CH<sub>2</sub>), 4.74 (s, 2H, NH<sub>2</sub>), 4.79 (s, 1H, CH), 7.13(d, H, H-Ar, *J* = 8.3), 7.17 (d-d, H, H-Ar, *J* = 2.15), 7.33(d, H, H-Ar, *J* = 2.05).



Scheme 2. Preparation of BaFe<sub>12</sub>O<sub>19</sub>@IM nanocomposite

**2-Amino-4-(4-methoxyphenyl)-7,7-dimethyl-5-oxo-5,6,7,8-tetrahydro-4H-chromene-3-carbonitrile (4j)** White crystalline solid. m.p.: 199–201 °C. <sup>1</sup>HNMR (500 MHz, CDCl<sub>3</sub>, 25 °C): δ = 1.02 (s, 3H, CH<sub>3</sub>), 1.09 (s, 3H, CH<sub>3</sub>), 2.25 (s, 2H, CH<sub>2</sub>), 2.43 (s, 2H, CH<sub>2</sub>), 3.75 (s, 3H, O-CH<sub>3</sub>), 4.34 (s, 1H, CH), 4.56 (s, 2H, NH<sub>2</sub>), 6.81 (d, 2H, H-Ar, *J* = 8.65 Hz), 7.14 (d, 2H, H-Ar, *J* = 8.65 Hz).

**7-Amino-5-(4-chlorophenyl)-2,4-dioxo-1,3,4,5-tetrahydro-2H-pyrido [2, 3-d]pyrimidine-6-carbonitrile (4q)** white crystalline solid. m.p.: 230 °C. <sup>1</sup>H NMR (500 MHz, DMSO-d<sub>6</sub>): δ = 4.24 (s, 1H, CH), 7.15 (s, 2H, NH<sub>2</sub>), 7.23 (d, *J* = 5 Hz, 2H, Ar-), 7.34 (d, *J* = 10 Hz, 2H, Ar-H), 11.07 (s, 1H, NH), 12.08 (s, 1H, NH).

**Methyl 6-amino-5-cyano-2-methyl-4-phenyl-4H-pyran-3-carboxylate (4s)** White crystalline solid. m.p.: 177–178 °C. <sup>1</sup>HNMR (500 MHz, CDCl<sub>3</sub>, 25 °C): δ = 3.31 (s, 3H, CH<sub>3</sub>), 3.58 (s, 3H, CH<sub>3</sub>), 4.17 (s, 1H, CH), 7.13–7.28 (m, 5H, H-Ar and NH<sub>2</sub>).

## Evaluation of antibacterial activities

The antibacterial activities of samples were measured using disc diffusion method. Two different bacterial strains, *E. coli*, and *S. aureus*, were cultured in Müeller-Hinton broth Agar using a sterile loop and incubated at 37 °C for 24 h before the test. The inoculum turbidity was standardized to equivalent of a 0.5 McFarland standard. Disc-shaped samples of samples with 1 cm<sup>2</sup> dimension were prepared and subjected to the inhibition zone tests. The discs were placed on culture plates. The diameter of the zones of growth inhibition around each disk was measured.

## Results and discussion

### Characterization of BaFe<sub>12</sub>O<sub>19</sub>@IM magnetic nanocomposites

The synthesized nanocomposites were characterized by FT-IR spectroscopy, EDX analysis, XRD pattern, SEM image, and TGA analysis. The FT-IR spectra of the IM, BaFe<sub>12</sub>O<sub>19</sub> nanoparticles and BaFe<sub>12</sub>O<sub>19</sub>@IM nanocomposite are shown in Fig. 1. The peak at 842.4 cm<sup>-1</sup> is related to the α(1,3) D-galactose C–O–S stretching vibrations. The C–O and C–OH stretching vibrations observed around 1010–1065 cm<sup>-1</sup>, also the S–O asymmetric sulfate stretching exhibited at 1249 cm<sup>-1</sup>. In addition to these peaks, the broadband stretching vibrations of hydroxyl groups appeared around 3400 cm<sup>-1</sup>. The OH bending vibration peaks become manifest at 1650.7 and 1537.6 cm<sup>-1</sup>. According to the BaFe<sub>12</sub>O<sub>19</sub> spectrum, the peaks at 426.1 and 584.0 cm<sup>-1</sup> are related to the metal-oxide stretching vibration emanated from the BaFe<sub>12</sub>O<sub>19</sub> crystalline structure. Furthermore, all depicted peaks above, the presence of the metal oxide peaks and biopolymer absorption bands, also exhibited in FT-IR of BaFe<sub>12</sub>O<sub>19</sub>@IM acknowledged that the chemical structure of the polysaccharide and BaFe<sub>12</sub>O<sub>19</sub> nanoparticles have been preserved after the heat treatments.

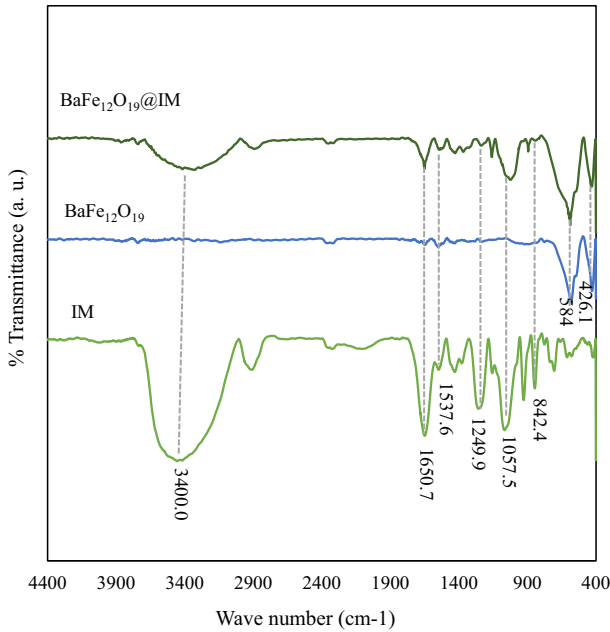


**Fig. 1** FTIR analysis of IM, the BaFe<sub>12</sub>O<sub>19</sub> nanoparticles, and BaFe<sub>12</sub>O<sub>19</sub>@IM nanocomposite

Thermal gravimetric analysis was achieved to assess the thermal stability and characteristic decomposition of IM and BaFe<sub>12</sub>O<sub>19</sub>/IM, from ambient to 600 °C at a heating rate of 10 °C/min, under air atmosphere (Fig. 2). As can be seen from Fig. 2, the TG curve of IM shows an initial weight loss (about 6%) from 50 to 170 °C which is due to the loss of moisture. The second degradation stage

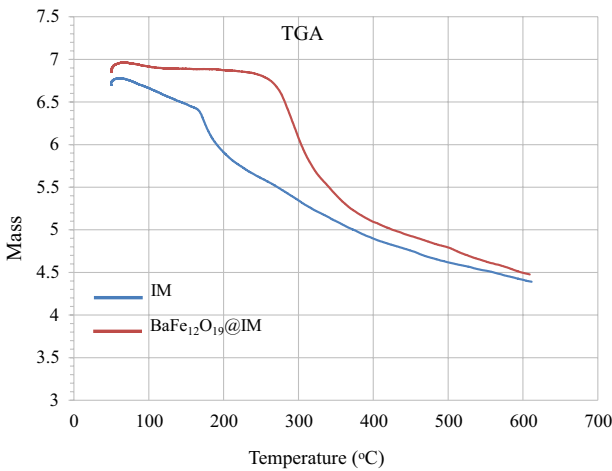


**Fig. 2** The thermogravimetric analysis of IM and BaFe<sub>12</sub>O<sub>19</sub>@IM

occurred in the range of 170–600 °C (ca. 30.0% weight loss) and may be attributed to the loss of sulfate group and also carbohydrate fragmentation. This result indicated that there remained many inorganic salts in IM. These results are in agreement with the previous studies carried out on the thermal behavior of carrageenan [44, 45]. For BaFe<sub>12</sub>O<sub>19</sub>/IM, around 30% weight loss occurred between 270 and 600 °C, indicating that BaFe<sub>12</sub>O<sub>19</sub>/IM exhibit better thermal stability than IM.

The magnetic properties of BaFe<sub>12</sub>O<sub>19</sub>@IM and BaFe<sub>12</sub>O<sub>19</sub> nanoparticles were investigated by VSM analysis with an applied field of ± 10 kOe at room temperature (Fig. 3). The VSM curve of the hard magnetic BaFe<sub>12</sub>O<sub>19</sub> discloses an intrinsic coercivity (H<sub>ci</sub>) of 5 kOe and the saturation magnetization of 48.60 emu/g. The magnetic hysteresis loops of BaFe<sub>12</sub>O<sub>19</sub>/IM nanocomposite indicated a decrease in H<sub>ci</sub> and the *M<sub>s</sub>* value, 2.5 kOe and 39.93 emu/g, respectively, due to the existence of polysaccharide in the composite. However, the magnetic property is at the appropriate level, to be easily separated from the reaction medium by an external magnet.

SEM images and EDS analysis of BaFe<sub>12</sub>O<sub>19</sub>, IM and BaFe<sub>12</sub>O<sub>19</sub>@IM nanocomposite are shown in Fig. 4a–c. The SEM image alongside with EDS analysis of BaFe<sub>12</sub>O<sub>19</sub> nanoparticles is presented in Fig. 4a. The SEM image revealed the hexagonal and lace-like morphology of synthesized BaFe<sub>12</sub>O<sub>19</sub>, while the EDS analysis of BaFe<sub>12</sub>O<sub>19</sub> showed the presence of Ba, Fe, O elements. The amorphous morphology of IM was revealed in SEM micrograph (Fig. 4b), beside the EDS analysis displaying the presence of O, C, and S elements in IM. The SEM image of BaFe<sub>12</sub>O<sub>19</sub>@IM nanocomposite showed uniform surface coverage of IM by hexagonal BaFe<sub>12</sub>O<sub>19</sub> nanoparticles presenting an average size of ~ 85 nm

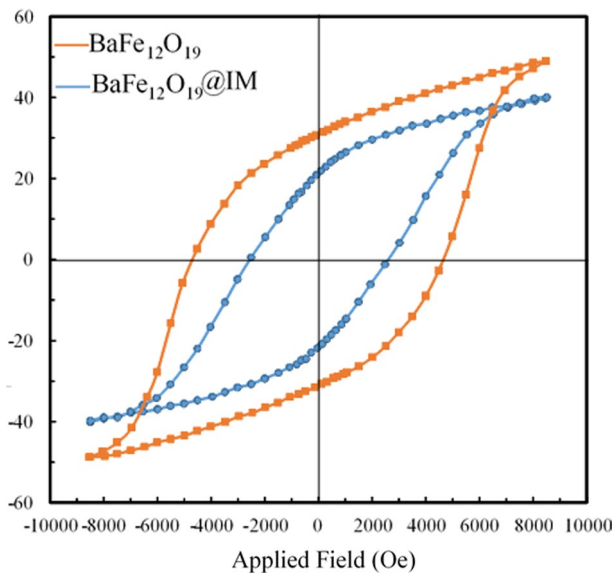


**Fig. 3** Magnetic hysteresis loops of the BaFe<sub>12</sub>O<sub>19</sub> nanoparticles and BaFe<sub>12</sub>O<sub>19</sub>@IM nanocomposite +

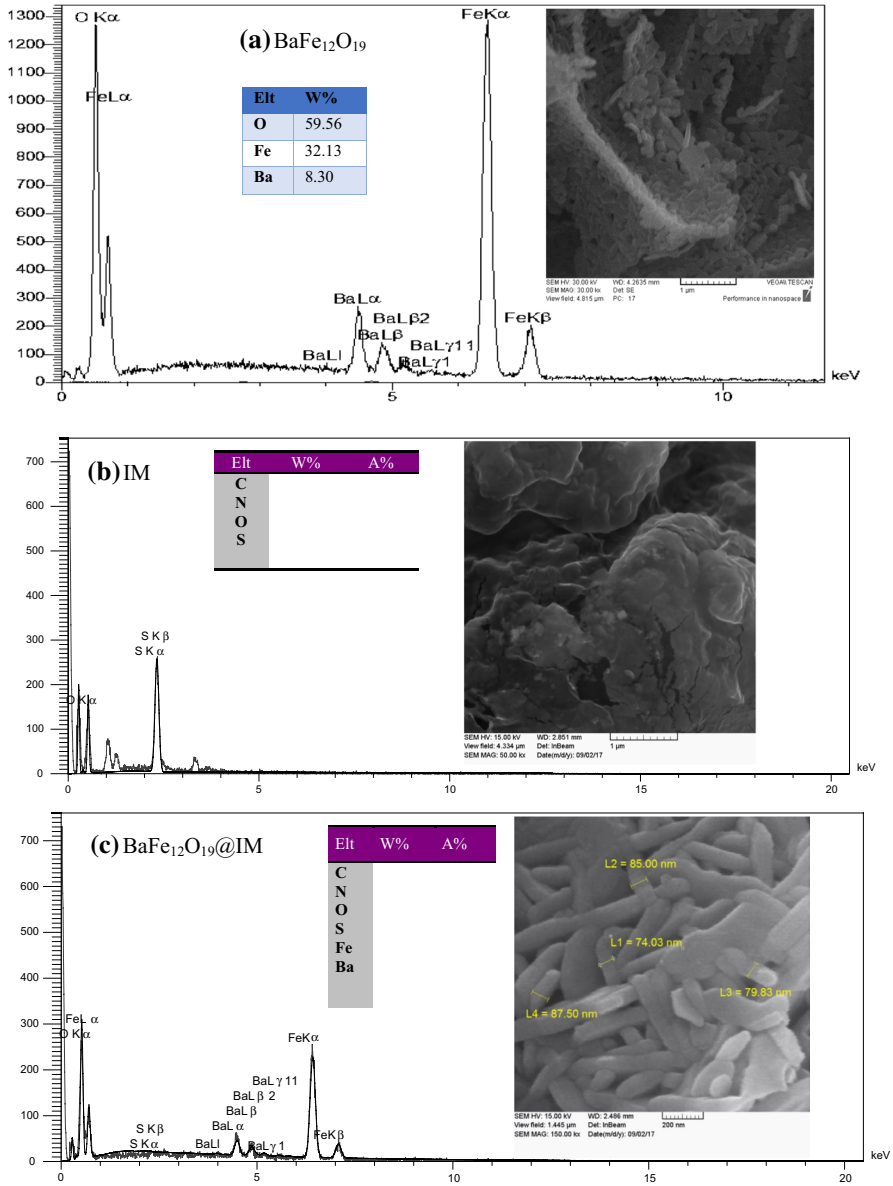


**Fig. 4** SEM images and the EDX analysis of **a** BaFe<sub>12</sub>O<sub>19</sub>@IM, **b** IM and **c** BaFe<sub>12</sub>O<sub>19</sub>@IM nanocomposite

(Fig. 4c). The EDS analysis of BaFe<sub>12</sub>O<sub>19</sub>@IM nanocomposite revealed the presence of both IM and BaFe<sub>12</sub>O<sub>19</sub> nanoparticles. Spectrum shows expected major elements such as Ba, Fe, O but also C and S (Fig. 4c).

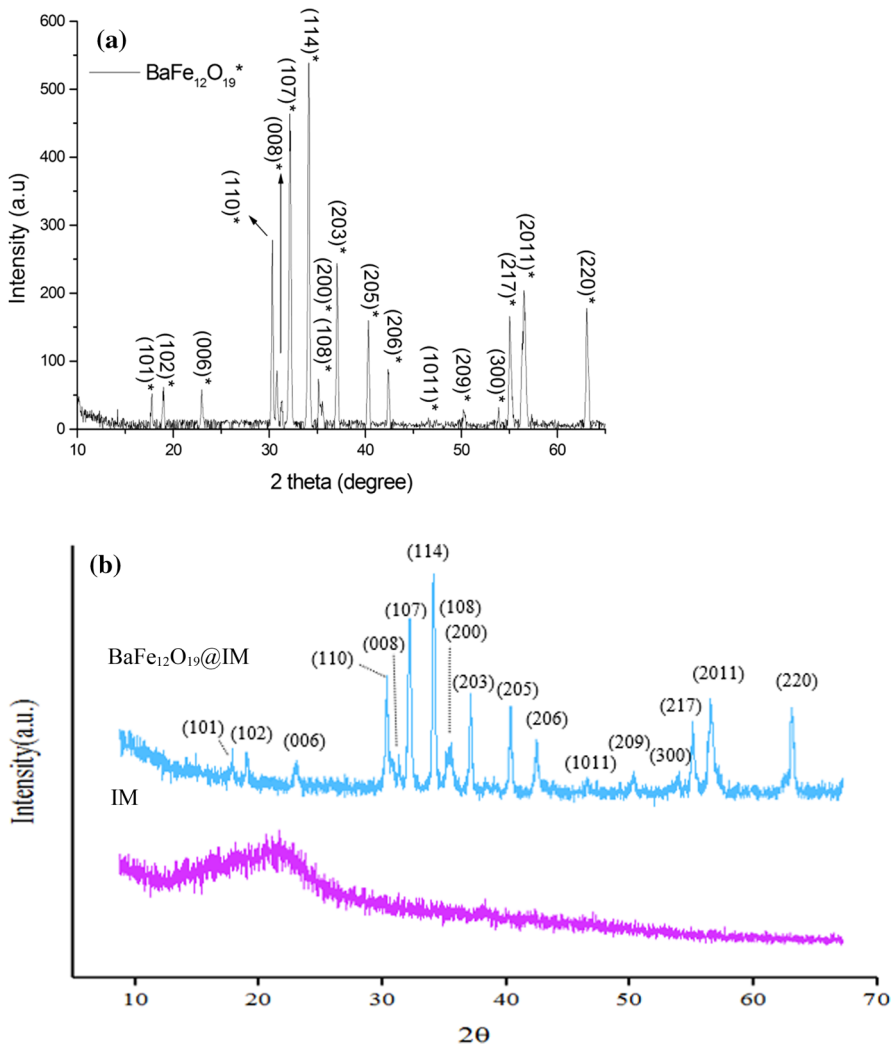


**Fig. 5** X-ray diffraction patterns of **a** the bare  $\text{BaFe}_{12}\text{O}_{19}$  and **b**  $\text{BaFe}_{12}\text{O}_{19}$ @IM and IM

X-ray diffraction patterns of the bare  $\text{BaFe}_{12}\text{O}_{19}$ ,  $\text{BaFe}_{12}\text{O}_{19}$ @IM, and IM are shown in Fig. 5. The diffraction peaks observed at  $2\theta$  values of 29.92, 31.68, 33.54, 34.84, 36.54, 54.61, 56.18, and 62.84 correspond to the crystal planes (110), (107), (114), (203), (217), (2011), and (220) and confirmed that  $\text{BaFe}_{12}\text{O}_{19}$  nanoparticles were synthesized in hexagonal crystal system based on the standard XRD pattern (JCPDS, card number 01-072-0738). According to the Scherrer equation, the size of the nanoparticles was 85 nm. The XRD pattern of IM displays a bump at  $2\theta$  around 22 which are referred to the amorphous nature of IM (Fig. 5b). The XRD pattern of  $\text{BaFe}_{12}\text{O}_{19}$ @IM nanocomposite indicates that the crystal structure of barium hexaferrite has been preserved after modification, and

at the same time, the existence of a small bump in  $2\theta$  around 22 might confirm the presence of IM in nanocomposite.

For the overall study of the catalytic property of BaFe<sub>12</sub>O<sub>19</sub>@IM magnetic nanocomposites, at first, the synthesis of the pyrans derivatives was optimized by the reaction of 4-methoxy benzaldehyde, malononitrile, and dimedone as a model reaction. To check the effect of the amount of catalyst, the reaction launched using a different amount of the BaFe<sub>12</sub>O<sub>19</sub>@IM (5, 10, 12, 15 mg) under certain reaction condition. Increasing the amount of catalyst from 5 to 12 mg resulted in a moderate improvement in the yield of the model reaction. Nevertheless, a higher amount of catalyst did not lead to a significant increase in yields. Thus, 12 mg of catalyst is sufficient for the synthesis of pyran annulated compounds with high yields. The model reaction has been studied in various protic and aprotic solvents such as ethanol, water, chloroform, and toluene. Ethanol has proved to be the best solvent for this reaction. The effect of temperature was also tested for the model reaction at three different temperatures: room temperature, 50 °C, and reflux conditions. As shown in Table 1, by raising the temperature from room temperature to reflux temperature, the reaction yield was improved. Optimum circumstances were achieved in refluxing ethanol, in the presence of 12 mg of catalyst. The reaction was unsuccessful in the absence of catalyst, but the results obtained through the separate use of IM and BaFe<sub>12</sub>O<sub>19</sub> showed the synergistic effect of the nanoparticles and the sulfated polysaccharide.

A series of pyrans were synthesized under reflux conditions in the presence of 12 mg catalyst. Different type of aromatic aldehydes containing electron

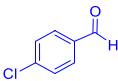
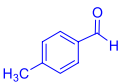
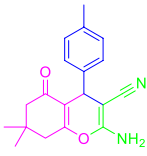
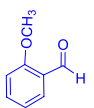
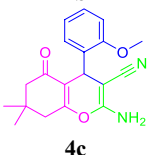
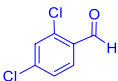
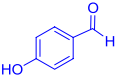
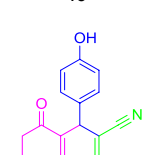
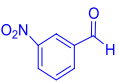
**Table 1** Optimization of the catalyst and the solvent amounts for the synthesis of pyrans heterocyclic compounds

| Entry | Temperature (°C) | Solvent       | Catalyst loading (mg)                          | Time (min) | Yield <sup>a</sup> (%) |
|-------|------------------|---------------|--|------------|------------------------|
| 1     | Reflux           | Ethanol       | BaFe <sub>12</sub> O <sub>19</sub> @IM (5 mg)  | 50         | 80                     |
| 2     | Reflux           | Ethanol       | BaFe <sub>12</sub> O <sub>19</sub> @IM (10 mg) | 35         | 85                     |
| 3     | Reflux           | Ethanol       | BaFe <sub>12</sub> O <sub>19</sub> @IM (12 mg) | 15         | 95                     |
| 4     | Reflux           | Ethanol       | BaFe <sub>12</sub> O <sub>19</sub> @IM (15 mg) | 15         | 95                     |
| 5     | r.t              | Water         | BaFe <sub>12</sub> O <sub>19</sub> @IM (12 mg) | 25         | 70                     |
| 6     | Reflux           | Chloroform    | BaFe <sub>12</sub> O <sub>19</sub> @IM (12 mg) | 40         | 55                     |
| 7     | Reflux           | Ethanol/water | BaFe <sub>12</sub> O <sub>19</sub> @IM (12 mg) | 20         | 85                     |
| 8     | Reflux           | Toluene       | BaFe <sub>12</sub> O <sub>19</sub> @IM (12 mg) | 60         | 55                     |
| 9     | r.t              | Ethanol       | BaFe <sub>12</sub> O <sub>19</sub> @IM (12 mg) | 35         | 70                     |
| 10    | 50               | Ethanol       | BaFe <sub>12</sub> O <sub>19</sub> @IM (12 mg) | 30         | 80                     |
| 11    | Reflux           | Ethanol       | IM (12 mg)                                     | 20         | 85                     |
| 12    | Reflux           | Ethanol       | BaFe <sub>12</sub> O <sub>19</sub> (12 mg)     | 45         | 65                     |
| 13    | Reflux           | Ethanol       | –  | 120        | 30                     |

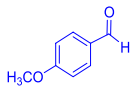
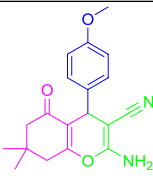
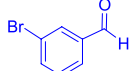
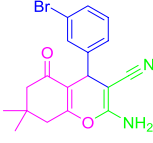
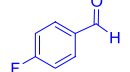
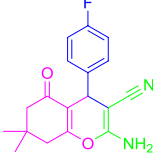
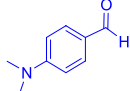
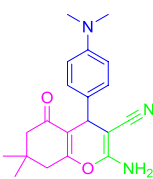
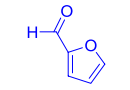
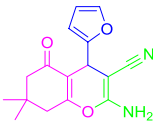
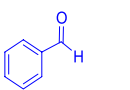
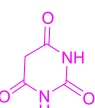
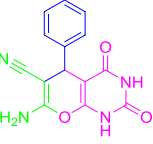
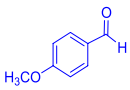
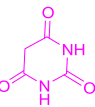
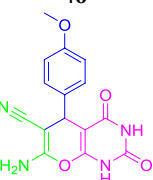
Model reaction conditions: 4-methoxy benzaldehyde (1 mmol), dimedone (1 mmol), malononitrile (1 mmol)

<sup>a</sup>Isolated yields

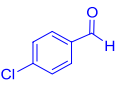
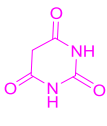
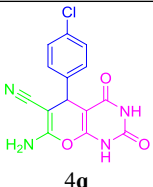
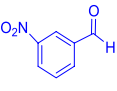
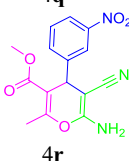
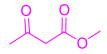
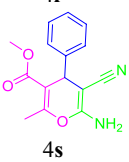
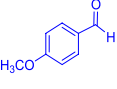
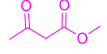
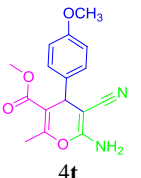
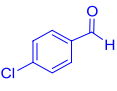
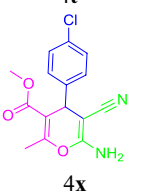
**Table 2** One-pot synthesis of pyran derivatives with BaFe<sub>12</sub>O<sub>19</sub>@IM magnetic nanocomposites

| Entry | Aldehyde  | C-H acid  | Product  | Time (min) | Yield (%) | m.p. (°C)                  |
|-------|---|---|--|------------|-----------|----------------------------|
|       |   |   |  |            |           | cal./ref.                  |
| 1     |    |    | <br><b>4a</b>   | 10         | 97        | 213–215<br>208–210<br>[47] |
| 2     |    |    | <br><b>4b</b>   | 20         | 81        | 213–216<br>210–213<br>[36] |
| 3     |    |    | <br><b>4c</b>   | 15         | 92        | 196–194<br>202–203<br>[48] |
| 4     |    |    | <br><b>4d</b>   | 10         | 95        | 180–183<br>192–194<br>[49] |
| 5     |   |   | <br><b>4e</b>  | 20         | 88        | 228–232<br>230–232<br>[32] |
| 6     |  |  | <br><b>4f</b> | 15         | 90        | 216–215<br>210–214<br>[50] |
| 7     |  |  | <br><b>4i</b> | 15         | 87        | 208<br>209–211<br>[51]     |

**Table 2** (continued)

|    |   |   |   |    |    |                            |
|----|---|---|---|----|----|----------------------------|
| 8  |    |    |    | 15 | 95 | 199–201<br>202–203<br>[36] |
| 9  |    |    |    | 15 | 92 | 228–231<br>228–230<br>[52] |
| 10 |    |    |    | 15 | 94 | 187–190<br>181–182<br>[53] |
| 11 |    |    |    | 15 | 87 | 216–218<br>217–218<br>[54] |
| 12 |  |  |   | 15 | 85 | 215–219<br>222–224<br>[33] |
| 13 |  |  |  | 15 | 90 | 275–278<br>278–279<br>[55] |
| 14 |  |  |  | 15 | 92 | 272–274<br>266–270<br>[50] |

**Table 2** (continued)

|    |   |   |  |    |    |                            |
|----|---|---|--|----|----|----------------------------|
| 15 |  |  |   | 10 | 95 | 230<br>228–230<br>[56]     |
| 16 |  |  |   | 15 | 89 | 200–202<br>204–206<br>[57] |
| 17 |  |  |   | 15 | 93 | 178<br>176<br>[58]         |
| 18 |  |  |   | 15 | 94 | 151–153<br>149<br>[58]     |
| 19 |  |  |  | 15 | 97 | 161–164<br>160–163<br>[59] |

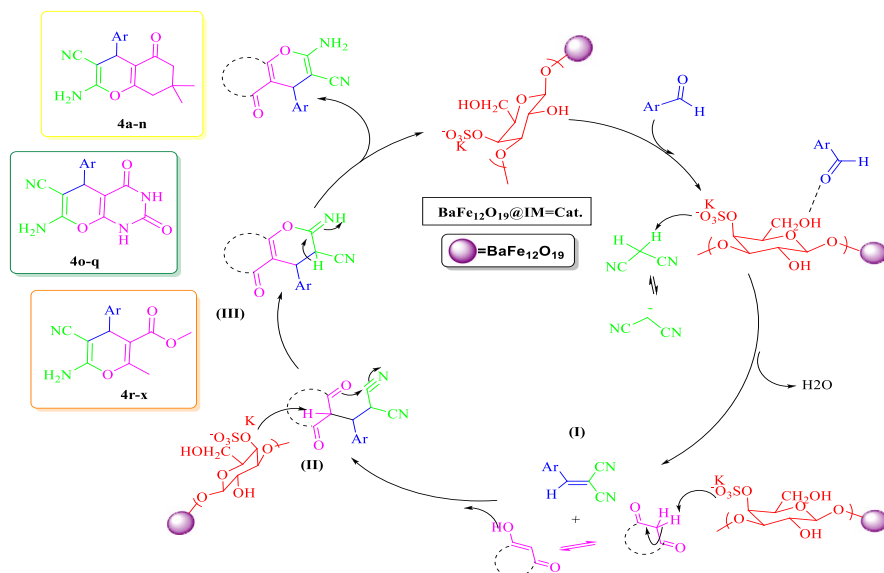
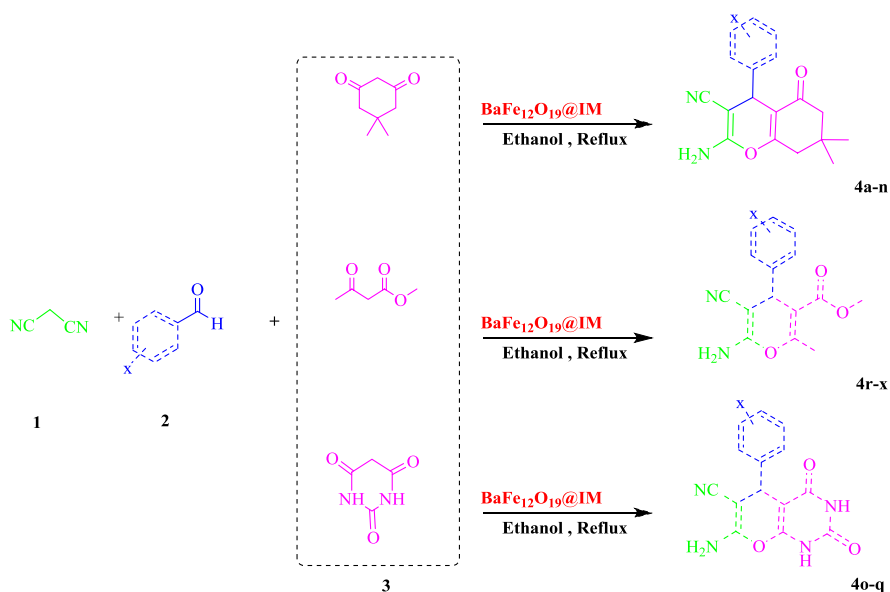
Reaction conditions: benzaldehyde derivatives (1 mmol), dimedone or malonylurea or methyl acetoacetate (1 mmol), malononitrile (1 mmol), BaFe<sub>12</sub>O<sub>19</sub>@ IM magnetic (12 mg) as a catalyst, in EtOH under reflux

**Table 3** Comparison of the present with some literature reported the synthesis of 4*H*-pyrans in the presence of the different catalyst

| Entry | Catalyst                                       | Conditions              | Yield (%) | Time      | Ref       |
|-------|--|-------------------------|-----------|-----------|-----------|
| 1     | Hydroxyapatite or modified sodium apatite      | Solvent free, r.t       | 61–96     | 2–6 h     | [60]      |
| 2     | MNP-DMAP                                       | Solvent free            | 96        | 1–3 h     | [61]      |
| 3     | FSM-16/AEPC-SO <sub>3</sub> H                  | Solvent free, 120 °C    | 88        | 15 min    | [62]      |
| 4     | WEMFSA   | EtOH, r.t               | 92        | 45 min    | [36]      |
| 5     | MCM-41@Schiff-based- Co(OAc) <sub>2</sub>      | H <sub>2</sub> O, 50 °C | 93        | 3 h       | [33]      |
| 6     | MgFe <sub>2</sub> O <sub>4</sub> nanoparticles | EtOH, 65 °C             | 74–92     | 10–15 min | [63]      |
| 7     | BaFe <sub>12</sub> O <sub>19</sub> @ IM        | Reflux in EtOH          | 96        | 15 min    | This work |

withdrawing and electron releasing substituent were used successfully in the reaction providing the corresponding products in high yield (Table 2).

In addition, the current green protocol is compared with other published reports in the literature for the synthesis of pyran derivatives (Table 3). The  $\text{BaFe}_{12}\text{O}_{19}@$



**Scheme 3.** Proposed mechanism for the synthesis of 2-Amino-3-cyano-4H-pyrans (4H-chromene-3-carbonitriles, 4H-pyran-3-carbonitriles, 2H-pyrano[2,3-d]pyrimidine-6-carbonitrile derivatives)

IM catalyst offers several advantages over some previous reported methods such as lower reaction time, simple work-up procedure, and higher performance.

The proposed mechanism for the synthesis of pyrans based on the literature [32, 62] is shown in Scheme 3. According to this mechanism, the arylidene malononitrile intermediate (I) was firstly formed by Knoevenagel condensation reaction between aldehyde and malononitrile in the presence of the  $\text{BaFe}_{12}\text{O}_{19}@IM$ . The intermediate (I) reacts with activated C–H acid compounds such as dimedone, malonylurea or methyl acetoacetate giving rise to the intermediate (II) which leads to the desired product after cyclization.

Catalyst recycling possibility has also been investigated. For this purpose, the magnetic  $\text{BaFe}_{12}\text{O}_{19}@IM$  nanocatalyst was removed from the reaction mixture by an external magnet, washed with ethanol, and then dried at room temperature. Subsequently, the recycled catalyst was reused in subsequent experiments. The results showed that the catalyst could be used successfully in six consecutive cycles without remarkable change in its catalytic activity (Fig. 6).

### The antimicrobial activity of $\text{BaFe}_{12}\text{O}_{19}@IM$ and 2-amino-4-(4-chlorophenyl)-7,7-dimethyl-5-oxo-5,6,7,8-tetrahydro-4H-chromene-3-carbonitrile (**4a**)

The antibacterial activity of  $\text{BaFe}_{12}\text{O}_{19}@IM$  and 2-amino-4-(4-chlorophenyl)-7,7-dimethyl-5-oxo-5,6,7,8-tetrahydro-4H-chromene-3-carbonitrile (**4a**) was also investigated against gram-positive bacteria *S. aureus* and gram-negative bacteria *E. coli*. The plate of Mueller-Hinton (MH) supplemented with Tween 80 surfactants (final concentration of 0.05% v/v) using agar medium was applied. Suspensions of each bacterium were accumulated to obtain in the vicinity of 108 colony-forming units (cfu) per mL for agar plating. For this purpose, an amount of 50 mg of the sample is to be examined. Then, for 2 h it was maintained at 4 °C and afterward was incubated at 37 °C for overnight. The size of inhibition zones (clear rings) around the antimicrobial samples was measured in millimeters after overnight incubation. The results showed that both  $\text{BaFe}_{12}\text{O}_{19}@IM$  and product (**4a**) have inhibition activity against *S. aureus* (inhibition zone diameter 10 mm and 9 mm respectively), while it does not have any effect on *E. coli* (Figs. 7a, b, 8).

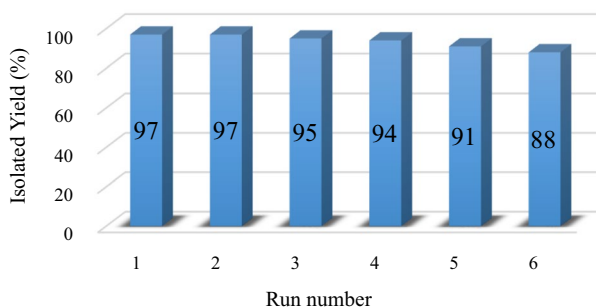


**Fig. 6** Catalyst reusability study showing the conversion and yield of products in model reaction

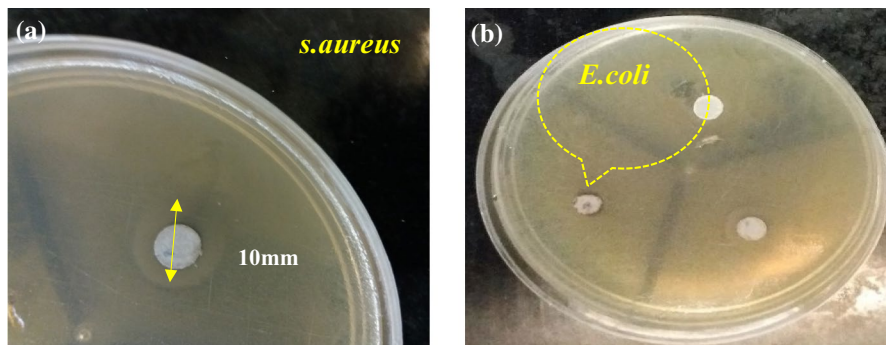


**Fig. 7** Antibacterial activity of  $BaFe_{12}O_{19}@IM$  against **a** *S. aureus* and **b** against *E. coli*

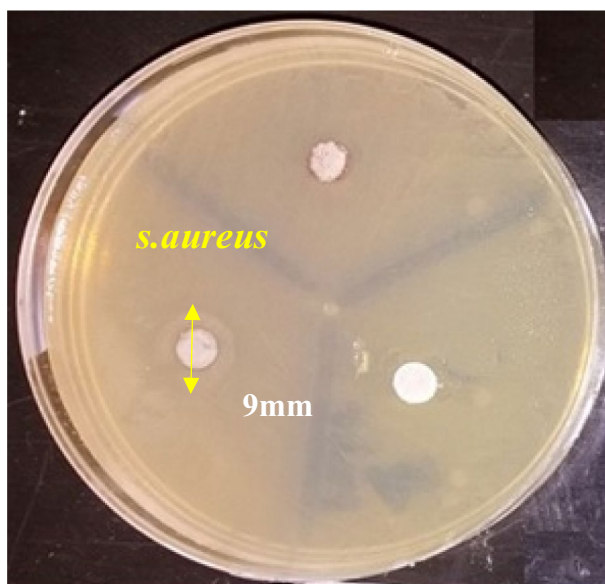


**Fig. 8** Antibacterial activity of 2-amino-4-(4-chlorophenyl)-7,7-dimethyl-5-oxo-5,6,7,8-tetrahydro-4H-chromene-3-carbonitrile (**4a**) against *S. aureus*

## Conclusions

In summary,  $BaFe_{12}O_{19}@IM$  magnetic bio-nanocomposites have been used as a novel and efficient heterogeneous catalyst in the synthesis of biologically active pyran derivatives. This heterogeneous bio-based catalyst has the promising potential to synthesize other heterocyclic compounds due to its unique features, precisely the reactive functional groups in its structure. Furthermore, a study on the antibacterial activity of  $BaFe_{12}O_{19}@IM$ , and the synthesized products, carried out on a bacterial strain, revealed that  $BaFe_{12}O_{19}@IM$  and

2-amino-4-(4-chlorophenyl)-7,7-dimethyl-5-oxo-5,6,7,8-tetrahydro-4*H*-chromene-3-carbonitrile (**4a**) have good antibacterial activity against gram-positive *Staphylococcus aureus*.

## Supporting information

<sup>1</sup>HNMR Spectral data of the selected products are shown in supporting information file.

**Acknowledgements** The authors wish to express their gratitude for the financial support provided by the Research Council of Iran University of Science and Technology (IUST), Tehran, Iran

## References

1. R.G. Saratale, G.D. Saratale, H.S. Shin, J.M. Jacob, A. Pugazhendhi, M. Bhaiare, G. Kumar, Environ. Sci. Pollut. Res. **25**, 10164 (2018)
2. A. Pugazhendhi, T.N.J.I. Edison, I. Karuppusamy, B. Kathirvel, Int. J. Pharm. **539**, 104 (2018)
3. S. Jeyarani, N.M. Vinita, P. Puja, S. Senthamilselvi, U. Devan, A.J. Velangani, M. Biruntha, A. Pugazhendhi, P. Kumar, J. Photochem. Photobiol. B **202**, 111715 (2020)
4. T. Parandhaman, N. Pentela, B. Ramalingam, D. Samanta, S.K. Das, ACS Sustain. Chem. Eng. **5**, 489 (2017)
5. Z. Jiang, K. Shan, J. Song, J. Liu, S. Rajendran, A. Pugazhendhi, J.A. Jacob, B. Chen, Life Sci. **220**, 156 (2019)
6. P.S. Murphin Kumar, S. Thiripuranthagan, T. Imai, G. Kumar, A. Pugazhendhi, S.R. Vijayan, ACS Sustain. Chem. Eng. **5**, 11290 (2017)
7. P.S.M. Kumar, V.K. Ponnusamy, K.R. Deepthi, G. Kumar, A. Pugazhendhi, H. Abe, J. Mater. Chem. A. **6**, 23435 (2018)
8. J. Kothandapani, S.S. Ganesan, Curr. Org. Chem. **23**, 313 (2019)
9. K.R. Reddy, P.A. Reddy, C.V. Reddy, N.P. Shetti, B. Babu, K. Ravindranadh, M.V. Shankar, M.C. Reddy, S. Soni, S. Naveen, Methods Microbiol. **46**, 227 (2019)
10. O. Zaitseva, D.A. Vinnik, E.A. Trofimov, Mater. Sci. Forum **946**, 186 (2019)
11. K. Watanabe, T. Fujihara, K. Watanabe, K. Kakizaki, K. Kamishima, J. Phys. Soc. Jpn. **89**, 014704 (2020)
12. D. Vinnik, F. Podgornov, N. Zabeivorota, E. Trofimov, V. Zhivulin, A. Chernukha, M. Gavrilyak, S. Gudkova, D. Zherebtsov, A. Ryabov, J. Magn. Magn. Mater. **498**, 166190 (2020)
13. S. Dagar, A. Hooda, S. Khasa, M. Malik, J. Alloys Compd. **826**, 154214 (2020)
14. T. Piri, R. Peymanfar, S. Javanshir, S. Amirnejat, Catal. Lett. **149**, 3384 (2019)
15. S. Amirnejat, A. Nosrati, S. Javanshir, M.R. Naimi-Jamal, Int. J. Biol. Macromol. **152**, 834 (2020)
16. C. Chellapandian, B. Ramkumar, P. Puja, R. Shanmuganathan, A. Pugazhendhi, P. Kumar, Process Biochem. **80**, 58 (2019)
17. M. Srinivasan, M. Venkatesan, V. Arumugam, G. Natesan, N. Saravanan, S. Murugesan, S. Ramachandran, Process Biochem. **80**, 197 (2019)
18. M. Venkatesan, V. Arumugam, R. Pugalendi, K. Ramachandran, K. Sengodan, S.R. Vijayan, U. Sundaresan, Process Biochem. **84**, 196 (2019)
19. B. Hemmati, S. Javanshir, Z. Dolatkah, RSC Adv. **6**, 50431 (2016)
20. R. Prabhu, R. Mohamed Asik, R. Anjali, G. Archunan, N.M. Prabhu, A. Pugazhendhi, N. Suganthi, Process Biochem. **84**, 39 (2019)
21. A. Maleki, Z. Hajizadeh, Silicon Chem. **11**, 2789 (2019)
22. E. Pourian, S. Javanshir, Z. Dolatkah, S. Molaie, A. Maleki, ACS Omega **3**, 5012 (2018)
23. F. Norouzi, S. Javanshir, BMC Chem. **14**, 1 (2020)
24. D. Kumar, P. Sharma, H. Singh, K. Nepali, G.K. Gupta, S.K. Jain, F. Ntie-Kang, RSC Adv. **7**, 36977 (2017)

25. K. Niknam, A. Piran, *Green Sustain. Chem.* **3**, 1 (2013)
26. D. Armesto, W.M. Horspool, N. Martin, A. Ramos, C. Seoane, *J. Org. Chem.* **54**, 3069 (1989)
27. G. Reynolds, K.H. Drexhage, *Opt. Commun.* **13**, 222 (1975)
28. N. Gouault, J.-F. Cupif, A. Sauleau, M. David, *Tetrahedron Lett.* **41**, 7293 (2000)
29. E.A.A. Hafez, M.H. Elnagdi, A.G.A. Elagamey, F.M.A.A. El-Taweel, *Heterocycles* **26**, 903 (1987)
30. P. Rai, A. Ibad, H. Sagir, I. Siddiqui, *ChemistrySelect.* **1**, 1300 (2016)
31. A. Maleki, Z. Varzi, F. Hassanzadeh-Afruzi, *Polyhedron* **171**, 193 (2019)
32. M.S. Esmaili, M.R. Khodabakhshi, A. Maleki, Z. Varzi, *Polycycl. Aromat. Compd.* (2020). <https://doi.org/10.1080/10406638.2019.1708418>
33. S. Pan, P. Li, G. Xu, J. Guo, L. Ke, C. Xie, Z. Zhang, Y. Hui, *Res. Chem. Intermed.* **46**, 1353 (2020)
34. A. Khazaei, F. Gholami, V. Khakyzadeh, A.R. Moosavi-Zare, J. Afsar, *RSC Adv.* **5**, 14305 (2015)
35. M.T. Maghsoodlou, N. Hazeri, M. Lashkari, F.N. Shahrokhbadi, B. Naghsbandi, M.S. Kazemidoost, M. Rashidi, F. Mir, M. Kangani, S. Salahi, *Res. Chem. Intermed.* **41**, 6985 (2015)
36. P.B. Hiremath, K. Kantharaju, *ChemistrySelect.* **5**, 1896 (2020)
37. M.S. Samuel, S. Jose, E. Selvarajan, T. Mathimani, A. Pugazhendhi, *J. Photochem. Photobiol. B.* **202**, 111642 (2020)
38. A. Pugazhendhi, D. Prabakar, J.M. Jacob, I. Karuppusamy, R.G. Saratale, *Microb. Pathog.* **114**, 41–45 (2018)
39. E. Tacconelli, E. Carrara, A. Savoldi, S. Harbarth, M. Mendelson, D.L. Monnet, C. Pulcini, G. Kahlmeter, J. Kluytmans, Y. Carmeli, *Lancet Infect. Dis.* **18**, 318 (2018)
40. M. Saravanan, S.K. Barik, D. MubarakAli, P. Prakash, A. Pugazhendhi, *Microb. Pathog.* **116**, 221 (2018)
41. A. Pugazhendhi, S.S. Kumar, M. Manikandan, M. Saravanan, *Microb. Pathog.* **122**, 84 (2018)
42. P. Nallasamy, T. Ramalingam, T. Nooruddin, R. Shanmuganathan, P. Arivalagan, S. Natarajan, *Process Biochem.* **92**, 355 (2020)
43. E. Nazarzadeh Zare, R. Jamaledin, P. Naserzadeh, E. Afjeh-Dana, B. Ashtari, M. Hosseinzadeh, R. Vecchione, A. Wu, F.R. Tay, A. Borzacchiello, P. Makvandi, *Appl. Mater. Interfaces* **12**, 3279 (2019)
44. K. Gold, B. Slay, M. Knackstedt, A.K. Gaharwar, *Adv. Ther.* **1**, 3 (2018)
45. S. Ma, L. Chen, X. Liu, D. Li, N. Ye, L. Wang, *Int. J. Green Energy* **9**, 13–21 (2012)
46. W.A.K. Mahmood, M.M.R. Khan, T.C. Yee, *J. Phys. Sci.* **25**, 123 (2014)
47. A. Maleki, J. Rahimi, K. Valadi, *Nano Struct. Nano Objects* **18**, 100264 (2019)
48. A. Maleki, M. Aghaei, H.R. Hafizi-Atabak, M. Ferdowsi, *Ultrason. Sonochem.* **37**, 260 (2017)
49. M. Bakherad, F. Moosavi, A. Keivanloo, R. Doosti, E. Moradian, M. Armaghan, *Res. Chem. Intermed.* **45**, 2981 (2019)
50. M. Zabihzadeh, A. Omid, F. Shirini, H. Tajik, M.S.N. Langarudi, *J. Mol. Struct.* **1206**, 127730 (2020)
51. B. Maleki, O. Reiser, E. Esmailnezhad, H.J. Choi, *Polyhedron* **162**, 129 (2019)
52. S. Banerjee, A. Horn, H. Khatri, G. Sereda, *Tetrahedron Lett.* **52**, 1878 (2011)
53. M. Honarmand, A. Tzani, A. Detsi, *J. Iran. Chem. Soc.* **16**, 571 (2019)
54. S. Gao, C.H. Tsai, C. Tseng, C.-F. Yao, *Tetrahedron Lett.* **64**, 9143 (2008)
55. A.V. Chate, R.M. Dongre, M.K. Khaire, G.M. Bondle, J.N. Sangshetti, M. Damale, *Res. Chem. Intermed.* **44**, 6119 (2018)
56. A. Maleki, A.A. Jafari, S. Yousefi, *Carbohydr. Polym.* **175**, 409 (2017)
57. X.-S. Wang, Z.-S. Zeng, M.-M. Zhang, Y.-L. Li, D.-Q. Shi, S.-J. Tu, X.-Y. Wei, Z.-M. Zong, *J. Chem. Res. Synop.* **4**, 228 (2006)
58. N. Azizi, S. Dezfooli, M. Khajeh, M.M. Hashemi, *J. Mol. Liq.* **186**, 76 (2013)
59. I. Kharbanger, M.R. Rohman, H. Mecadon, B. Myrboh, *Int. J. Org. Chem.* **2**, 282 (2012)
60. A. Fihri, C. Len, R.S. Varma, A. Solhy, *Coord. Chem. Rev.* **347**, 48 (2017)
61. S.K. Dangolani, F. Panahi, M. Nourisefat, A. Khalafi-Nezhad, *RSC Adv.* **6**, 92316 (2016)
62. M. Hajjami, F. Gholamian, R.H. Hudson, A.M. Sanati, *Catal. Lett.* **149**, 228 (2019)
63. B. Eshtheadian, M. Rouhani, Z. Mirjafary, *J. Iran. Chem. Soc.* **17**, 469 (2020)